Available online at www.sciencedirect.com
ScienceDirect
Catalysis Today 119 (2007) 114–119
CATALYSIS TODAY
www.elsevier.com/locate/cattod

Interaction of NO and NO_2 with the surface of $Ce_xZr_{1-x}O_2$ solid solutions – Influence of the phase composition

Andrzej Adamski [a,*], Edyta Tabor [a,b], Barbara Gil [a], Zbigniew Sojka [a,c]

[a] *Jagiellonian University, Faculty of Chemistry, Ingardena 3, 30-060 Cracow, Poland*
[b] *PAS, Institute of Catalysis and Surface Chemistry, Niezapominajek 8, 30-239 Cracow, Poland*
[c] *Regional Laboratory of Physicochemical Analyses and Structural Research, Ingardena 3, 30-060 Cracow, Poland*

Available online 11 September 2006

Abstract

Structural (XRD) and spectroscopic (EPR, IR and Raman) investigations were performed to elucidate the influence of CeO_2 content on the phase composition and surface chemistry of $Ce_xZr_{1-x}O_2$ solid solutions ($x = 0.10$–0.85), interacting with NO and NO_2 in the absence and presence of oxygen. Strong influence of ceria loading on the adsorption modes of both nitrogen oxides and the nature of the resultant surface species was revealed. Adsorption of NO led to formation of mononitrosyl complexes, dimers and N_2O, whereas interaction of NO_2 with the ceria–zirconia catalyst resulted in the adsorbate disproportionation or coupling, depending on the sample composition.

Keywords: $Ce_xZr_{1-x}O_2$; Phase composition; NO_x adsorption; EPR; RS

1. Introduction

One of the most important industrial application of CeO_2–ZrO_2 solid solutions is related with the automobile three-way catalyst, where the support extensively assists in catalytic performance of the deposited active phase, constituted by noble metals such as Pt, Rh or Pd [1,2]. The redox properties of the solid solution, controlled by the CeO_2/ZrO_2 ratio and its phase composition [3], are intimately associated with easy oxygen shuttling between the catalyst and the gas phase under oxygen lean or rich conditions, respectively. The resultant oxygen storage capacity of $Ce_xZr_{1-x}O_{2-y}$ is directly related to facile reduction of cerium component, accompanied by concomitant creation of oxygen vacancies. Apart from playing the role of a good oxygen buffer, the CeO_2–ZrO_2 support can directly participate in the reduction of nitric oxides [4–6]. For instance, in the case of the three way catalyst, it has been found that at temperatures higher than 400 K, NO can be dissociatively adsorbed on the zirconia–ceria support, following a mechanism involving oxygen vacancies [6].

Paramagnetic NO and NO_2 molecules adsorbed on the surface of CeO_2–ZrO_2 solid solutions can play the role of probe molecules while examined by IR and EPR, providing important information not only about coordinatively unsaturated sites of different reducibility and acid–base properties [7–9], but also about occurrence of zirconia-enriched and ceria-enriched domains, which cannot be revealed by powder diffraction [10,11].

At temperatures below 1273 K, the CeO_2–ZrO_2 solid solutions may exist in three different phases, depending on the molar ratio of both oxide components. Thus, for CeO_2 contents lower than 10%, a monoclinic ($P2_1/c$) phase, whereas for CeO_2 contents higher than 80%, a cubic phase ($Fm3m$) have been identified [6,12]. In the intermediate concentration region, both stable (t) and metastable (t′ and t″) tetragonal phases ($P4_2/nmc$) have been postulated. The t′ structure can be derived from the cubic phase by the cation diffusionless phase transition, whereas the t″ phase characterized by the lattice parameter ratio $a/c = 1$, is an intermediate one between the tetragonal t′ and the cubic phase [6]. Actually, the phase boundaries are rather vague due to a fact that for the metastable tetragonal forms, distortions from the fluorite-type structure are rather easy and highly sensitive to particles size.

For bare ZrO_2 and zirconia-based materials, the stability of a particular polymorph is strongly size-dependent

* Corresponding author.
E-mail address: adamski@chemia.uj.edu.pl (A. Adamski).

0920-5861/$ – see front matter © 2006 Elsevier B.V. All rights reserved.
doi:10.1016/j.cattod.2006.08.003

($\Delta G(r < r_o)_{m\rightarrow t} = 4/3\pi r^3 \Delta G_{bulk} + 4\pi r^2(\gamma_t - \gamma_m) < 0$) [13,14]. The monoclinic form is much more stable than the tetragonal one, in the case of coarse-grained samples. However, if the particle size r is lower than the critical value of $r_o \sim 30$ nm [15], the tetragonal polymorph becomes thermodynamically more stable, because it exhibits considerably lower surface energy than the monoclinic counterpart ($\gamma_t < \gamma_m$).

The aim of present work was to characterize the $Ce_xZr_{1-x}O_2$ solid solutions of various compositions from the view point of their bulk and surface properties, to find the correspondence between the ceria content and the adsorption modes of NO and NO_2. Particular attention was devoted to the formation and thermal evolution of the resultant surface complexes and their reactivity with dioxygen.

2. Experimental

The investigated binary CeO_2–ZrO_2 solid solutions, containing 10–85 mol% CeO_2, were commercially produced by *RHODIA* by hydrothermal synthesis from nitrate precursors, dried at 373 K for 1 h and then calcined at 873 K for 6 h. The single phase zirconium and cerium dioxides, used in these studies as reference systems, were obtained from aqueous solutions of the corresponding $ZrOCl_2$ and $Ce(NO_3)_3{\cdot}6H_2O$ (Aldrich 99.99%) precursors by precipitation with 25% solution of ammonia. After drying, the samples were calcined in air at 873 K for 6 h.

The investigated samples were structurally and texturally characterized by XRD, SEM/TEM, and N_2-porosimetry. Their spectroscopic characterization by EPR, IR and Raman was also performed. X-ray diffraction patterns were recorded with Philips X'Pert (PW1710) diffractometer using monochromatized Cu Kα radiation. Raman spectra were measured by means of a FTS 6000 spectrometer equipped with a BIORAD accessory. The samples were excited with the 1064 nm line of a diode-pumped Nd:YAG laser (Spectra Physics Model T108S) and the scattered radiation was collected at 180°, using 4 cm^{-1} resolution. The IR spectra were registered with the resolution of 2 cm^{-1} using an Equinox 55 spectrometer equipped with a MCT detector. The samples placed in the IR cell on a silicon wafer were treated *in situ*. The CW-EPR X-band spectra were recorded at room and liquid nitrogen (77 K) temperatures with a Bruker ELEXSYS E-500 spectrometer operating at the 100 kHz field modulation. EPR parameters were determined by simulation using the EPRsim32 program [16].

In all cases described below, nitrogen oxides were adsorbed at pressure of 20 Torr (non-equilibrium pressure) on the samples previously outgassed under vacuum at $p \leq 10^{-5}$ Torr and activated at 623–673 K for 0.5 h. All samples were contacted with NO and NO_2 at 77 K for 1 min and next gradually exposed to room temperature or to 333 K, to follow the adsorption progress monitored by EPR. Once the NO_x evolution was accomplished, the samples were outgassed and oxygen was introduced under the pressure of 2 Torr at 77 K. The exposure to room temperature was then repeated.

3. Results and discussion

3.1. Phase composition analysis

Due to the strong mutual dependence between the bulk structure and the surface properties of the CeO_2–ZrO_2 solid solutions, a detailed phase analysis in the whole concentration range is an indispensable step of samples characterization. Introduction of less than 10 mol% of CeO_2 into m-ZrO_2 matrix did not involve any appreciable phase modification at room temperature. However, a phase transition was observed above 1470 K, when the monoclinic phase is transformed into the stable tetragonal form. The m → t phase transition can be followed easily by XRD, because the maxima corresponding to (1 1 1) and $(1\,1\,\bar{1})$ reflections, diagnostic of the monoclinic zirconia, were replaced by a single (1 1 1) reflection characteristic of the tetragonal phase. At CeO_2 loadings exceeding 10 mol%, metastabilization of the high-temperature tetragonal and cubic phases takes place already at room temperature. Thus, the (1 1 1) reflection of t-ZrO_2 was clearly visible in the diffraction pattern of the $Ce_{0.75}Zr_{0.25}O_2$ solid solution (Fig. 1a). Because the metastable tetragonal phase can exists in two t′ and t″ variants depending on the CeO_2 content [6], distinguishing between them required a detailed insight into XRD data in the 2θ region of 70–71.5° (Fig. 1a, inset). The (4 0 0) reflection, which is crucial for making the phase discrimination, splits into (0 0 4) and (4 0 0) components (usually for $0.20 \leq x \leq 0.65$) in the case of the t′ phase, or it remains intact (for $0.70 \leq x \leq 0.90$), when the t″ phase is dominant [5,12]. Due to the low sensitivity of the XRD method to small shifts in the position of oxygen atoms and relatively weak intensity of those lines, such analysis is rather difficult. Contrary to this, the nuances in the phase composition of the CeO_2–ZrO_2 solid solutions were much better pronounced in the Raman spectroscopy, which is more sensitive to the short-range oxygen displacement, owing to the large polarizability of oxygen ions. The factor group theoretical analysis predicts 18 ($9A_g + 9B_g$) Raman-active modes for the monoclinic ZrO_2 form, 6 ($A_{1g} + 2B_{1g} + 3E_g$) for the tetragonal one and only 1 F_{2g} mode for the cubic phase [17,18]. The number of components observed in the Raman spectra decreased continuously with CeO_2 loading, from at least 10 bands observable for $Ce_{0.10}Zr_{0.90}O_2$ (m), 8 for $Ce_{0.20}Zr_{0.80}O_2$ (m + t′), 4 for $Ce_{0.50}Zr_{0.50}O_2$ (t′) and $Ce_{0.70}Zr_{0.30}O_2$ (t″) to 1 band for $Ce_{0.85}Zr_{0.15}O_2$ (c), making the distinction between the t″ and cubic phases possible. The representative spectra, recorded for $Ce_xZr_{1-x}O_2$ solid solutions, with $x = 0.20$, 0.70 and 0.85, respectively are presented in Fig. 1b. They obviously differed in the number of resolved bands, but in all cases the most intense ones occurred between 465 and 490 cm^{-1}. A single band at 469 cm^{-1} observed for $Ce_{0.85}Zr_{0.15}O_2$ was attributed to the symmetrical F_{2g} mode, characteristic of the cubic phase with the fluorite-like structure. In the case of the solid solutions with an intermediate ceria content (but higher than 50 mol%), such as $Ce_{0.70}Zr_{0.30}O_2$, weaker bands at ~170 and 310 cm^{-1} along with a broad feature centered at ~632 cm^{-1} (A_{1g}), revealed the presence of the t″ phase. The last band is usually ascribed to

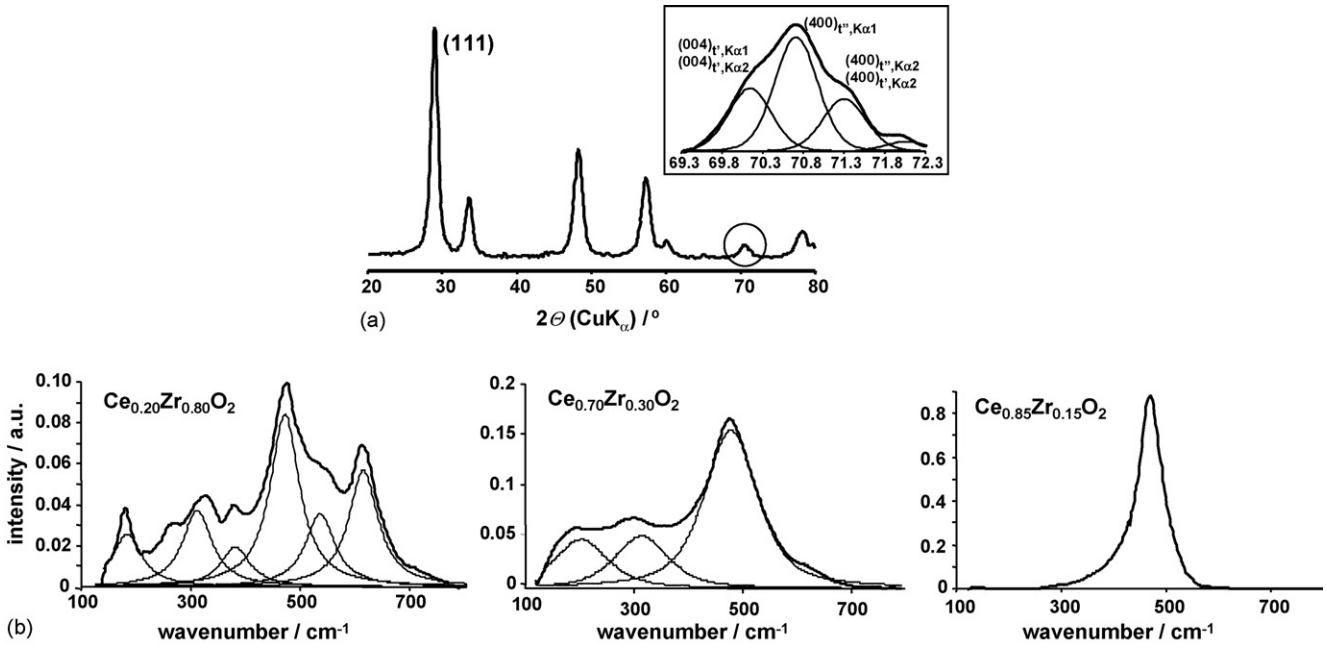

Fig. 1. Phase analysis for ceria–zirconia systems. (a) XRD pattern of $Ce_{0.75}Zr_{0.25}O_2$ system, in the inset deconvolution of the marked region is presented. (b) Raman spectra for $Ce_xZr_{1-x}O_2$, where $x = 0.20$, 0.70 and 0.85, respectively.

distortion in the fluorite structure due to the replacement of some Ce^{4+} cations by Zr^{4+} in the CeO_2 lattice. Several poorly resolved bands in the 150–400 cm^{-1} region along with an intense maximum at 621 cm^{-1} (A_g), appearing in the spectrum of $Ce_{0.20}Zr_{0.80}O_2$, imply the presence of a monoclinic polymorph. However, a peak at ~320 cm^{-1} (B_{1g}) indicated a minor contribution of the tetragonal t′ phase.

A shoulder at ca. 540 cm^{-1} visible in the Raman spectrum of $Ce_{0.20}Zr_{0.80}O_2$ solid solution is most probably due to luminescence of a trivalent lanthanide impurity. Such impurities are often present in ceria–zirconia materials and can strongly influence Raman spectra. In the case of the excitation with the 1064 nm line, no other luminescence bands, disturbing the recorded Raman spectra are expected [19].

The EPR spectra of the $Ce_xZr_{1-x}O_2$ solid solutions ($x = 0.1$–0.85) activated at 623–673 K in air, recorded at 77 K were rather weak and exhibited the presence of a narrow axial EPR signal around $g_{av} = 1.97$, without any appreciable hyperfine structure (Fig. 2, inset). In principle, it could be attributed to either Zr^{3+} ($4d^1$) or Ce^{3+} ($4f^1$) matrix defects, which both are paramagnetic. However, for cerium ions the spin-orbit coupling strongly dominates the crystal filed, resulting in a $^2F_{5/2}$ ground state the degeneracy of which is further weakly split by the local crystal field into three Kramers doublets. EPR transitions may occur only within the lowest doublet, and the corresponding EPR spectra being strongly affected by the fast spin-lattice relaxation will, therefore, require recording temperatures below 20 K to be observed Thus, at 77 K the signal due to Ce^{3+} is obviously beyond the detection limit. Following literature, we can then attribute the observed signal to Zr^{3+} defects reasonably [20]. Indeed, the concentration of those defects determined from the integral intensity of the EPR spectra decreased with lowering of the ZrO_2 content in the solid solutions. An alternative attribution of this signal to chromium impurities, proposed elsewhere [21,22] is less probable because its g factor is in our case slightly higher in comparison to the reported $g_{av} = 1.95$, and in addition no hyperfine structure due to ^{53}Cr nuclei ($I = 3/2$, 9.55%) was observed.

3.2. Adsorption of NO and NO_2

There are three principal NO chemisorption modes leading to the formation of surface mononitrosyl $\{M\text{-}NO\}^n$ complexes: a linear η^1-N coordination (often associated the nitrosonium cation NO^+), a bent η^1-N one (characteristic of the nitroside NO^- anion) and bridging η^2-N mode [23,24]. The bent structure is also assumed in the case of dimers or coupled mononitrosyls. Removal of the degeneracy of both π^* orbitals of the NO molecule ($^2\Pi_{1/2}$) upon adsorption, makes the resulting $\{M\text{-}NO\}^n$ complex EPR-active. The components of the corresponding orthorhombic g-tensor are given by the following equations: $g_x = g_e + 2(\lambda/\Delta) - (\lambda/\delta)^2 + (\lambda/\delta)(\lambda/\Delta)$, $g_y = g_e - (\lambda/\delta)^2 - (\lambda/\delta)(\lambda/\Delta)$ and $g_z = g_e - 2(\lambda/\delta) + (\lambda/\delta)^3$, where λ is the spin-orbit coupling constant, and Δ and δ are the crystal field splitting parameters [25].

Low-temperature (77 K) contact of the CeO_2–ZrO_2 solid solution with 20 Torr of NO led to distinct changes in the EPR spectra. In Fig. 2a and b representative results obtained for the ceria-lean (20 mol%) and the ceria-rich (85 mol%) samples are presented. Just after NO introduction, a broad ($\Delta B_{pp} \approx 20$ mT) asymmetric signal at $g_{iso} \approx 1.99$ appeared, regardless of the chemical composition of the samples. Its intensity was distinctly lower for $Ce_{0.85}Zr_{0.15}O_2$. Due to the poor resolution only traces of the ^{14}N ($I = 1$) hyperfine structure could be

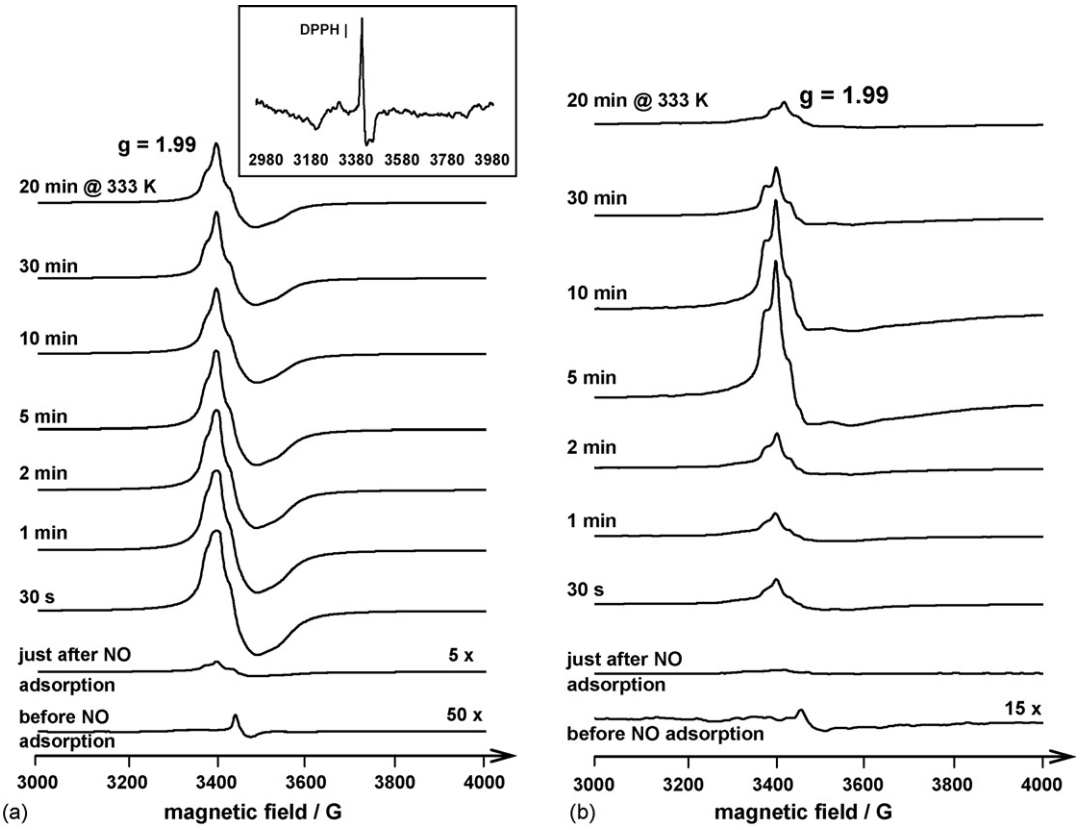

Fig. 2. EPR spectra of CeO_2–ZrO_2 systems before and after NO adsorption at 77 K, recorded at 77 K as a function of the time of exposure to RT and 333 K. CeO_2:ZrO_2 ratio in mol%: (a) 20:80 and (b) 85:15. In the inset the signal from Zr^{3+} defects is shown.

observed in some favorable cases. The signal is typical of loosely trapped NO radicals subjected to restricted motion on the surface. The presence of such NO species was also confirmed in parallel IR studies by the band at ~1865 cm^{-1}, which is very close to ν(N–O) stretching vibration of gaseous NO (1876 cm^{-1}) [26]. For the samples containing less than 50 mol% of CeO_2, the surface trapped NO predominated also at room temperature. In contrast, for the ceria-rich samples distinct $\{Ce–NO\}^1$ complexes with the characteristic nitrogen hyperfine structure were readily formed (Fig. 2b). Their EPR parameters are similar to those reported for $Ce_{0.75}Zr_{0.25}O_2$ [27], where the simultaneous presence of both isolated and coupled (dimeric) nitrosyls was revealed by computer simulation. Following the classification proposed by Astruc [28], the orthorhombic signal with $g_x = 1.997$, $g_y = 2.000$ and $g_z = 1.908$ and $|^{N}A_x|g\beta_e = 3.1$ mT can be attributed to a ligand centred radical complex $\{Ce–NO\}^1$.

The strong IR band at 1750 cm^{-1} indicates that the NO moiety should be bent, acquiring some partial negative charge ($NO^{\delta-}$) [29]. The occurrence of an additional weak band at 1185–1195 cm^{-1} at higher ceria loadings (e.g. 75 mol%) suggests the formation of strongly bent or even bridging (η^2-N,O) nitrosyl species [29]. Closer inspection of the EPR signal revealed that apart from the mononitrosyl complexes, surface dimers $(NO)_2$ were also formed. The characteristic fine structure features ($D \approx 22 \pm 1$ mT) originate from dipolar interaction between the unpaired electrons of the two adjacent NO molecules [30].

The NO adsorption progress as a function of the exposure time, followed by the integral intensity of the corresponding EPR spectrum, for the $Ce_{0.20}Zr_{0.80}O_2$ and $Ce_{0.85}Zr_{0.15}O_2$ solid solutions is shown in Fig. 3. Clearly, the formation of the paramagnetic nitrosyl complexes was much easier in the case of the monoclinic samples (with the maximum occurring within 60–90 s), whereas for the ceria-rich cubic samples, such maximum was shifted to 5 min. At elevated temperatures (333 K) and prolonged exposure (~20 min), part of the NO

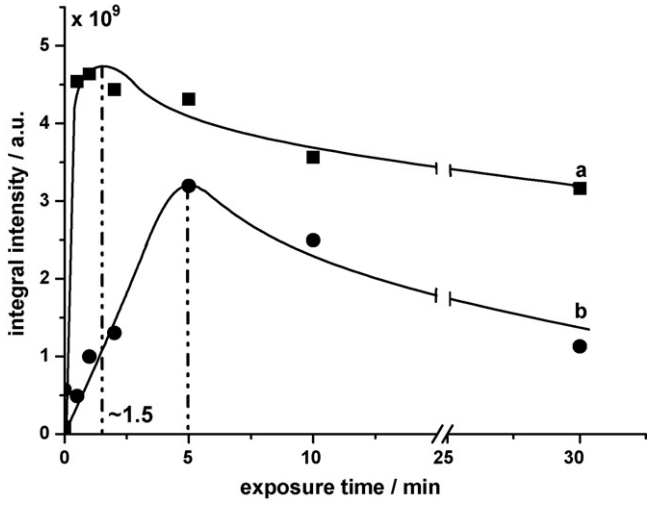

Fig. 3. Evolution of the intensity of the EPR spectra of NO/$Ce_xZr_{1-x}O_2$ as a function of time of exposure to RT. CeO_2:ZrO_2 ratio: (a) 20:80 and (b) 85:15.

molecules that remained on the surface is transformed into diamagnetic entities such as N_2O or $N_2O_2^{2-}$, giving rise to IR bands at ~2230 and 1300 cm^{-1}. For N_2O diagnostic bands at 2230 cm^{-1}, attributed to ν(N–N) streching mode and at 1285 cm^{-1}, ascribed to N–O stretching, are to be expected [29,31]. The corresponding N–N stretching band in *cis*-$N_2O_2^{2-}$ hyponitrates appears at 1314–1350 cm^{-1} and in *trans*-$N_2O_2^{2-}$ at 1419 cm^{-1}, whereas the symmetric and antisymmetric N–O modes at 1015–1057, 857–954 cm^{-1} (*cis*) and 1120, 1030–1105 cm^{-1} (*trans*) [4,29], respectively. Eventual attribution of those bands to surface hyponitrate or nitrous oxide species may pose some problems, because of a strong absorption of the CeO_2–ZrO_2 solid solutions in this region, and a relatively low intensity of the N–O vibration band. Nonetheless, the appearance of the IR maxima at 2230 and 1300 cm^{-1} speaks in favor of N_2O species, which could be produced in the following way: $2NO + O^{2-} \rightarrow N_2O + O_2^{2-}$.

Subsequent introduction of dioxygen at 77 K into the NO/$Ce_{0.85}Zr_{0.15}O_2$ system, previously outgassed, did not generate any new EPR signal. However, after exposing the sample to room temperature for 30 s a new intense signal appeared, which was attributed to O_2^- radical initially associated with Ce^{4+} cations and then stabilized on Zr^{4+} sites [27]. The progress of the reaction with oxygen was clearly connected with the population of the mononitrosyl species on the surface, which was found to be the highest on the ceria-rich samples. Decay of the surface-stabilized O_2^- radicals was rather fast, and diamagnetic peroxynitrates $[O_2N–O_2]^{2-}$ that further decompose into NO_3^- and O^{2-}, have been suggested by Martínez-Arias et al. to be the intermediates of such reaction [4]. The strong IR vibrations in the region 1295–1625 cm^{-1} and weak bands between 1020 and 1150 cm^{-1} support the formation of nitrates as final products of the reaction between adsorbed NO and O_2 [32–34].

Distinct differences in surface properties for the samples of various phase composition were also reflected in low-temperature adsorption of NO_2. As a stable 17-electron paramagnetic molecule, NO_2 should be detected in EPR quite easily. Surprisingly, the products of the surface reaction with ceria-rich samples were EPR silent. Only in the case of the $Ce_{0.10}Zr_{0.90}O_2$ and $Ce_{0.20}Zr_{0.80}O_2$ samples (after heating to 333 K for 5 min) an EPR signal with $g_{av} \approx 1.99$ was observed upon NO_2 adsorption (Fig. 4a). This signal was very similar to that obtained previously for NO interacting with the $Ce_{0.20}Zr_{0.80}O_2$ solid solution. Apparently on the surface of the monoclinic polymorph, nitrogen dioxide disproportionates into NO and NO_3^- similarly as it was described earlier for NO_2/BaO system [35]. This process can be written as $2NO_2 + Ce^{3+} \rightarrow \{Ce–NO\}^1 + NO_3^-$ in accordance with the appearance of strong IR bands at ~1740 cm^{-1}, 1700 and 1255 cm^{-1} (Fig. 4b) assigned to the surface nitrosyl and nitrate species, respectively. A broad peak at 1185 cm^{-1} also appearing in the IR spectrum was attributed to bridging NO. Contrary to the dissociative adsorption on the samples with low ceria content, in the case of $Ce_{0.85}Zr_{0.15}O_2$ the IR investigation revealed an associative adsorption resulting in coupling of NO_2, as it can be judged from the appearance of a strong band at 750 cm^{-1}

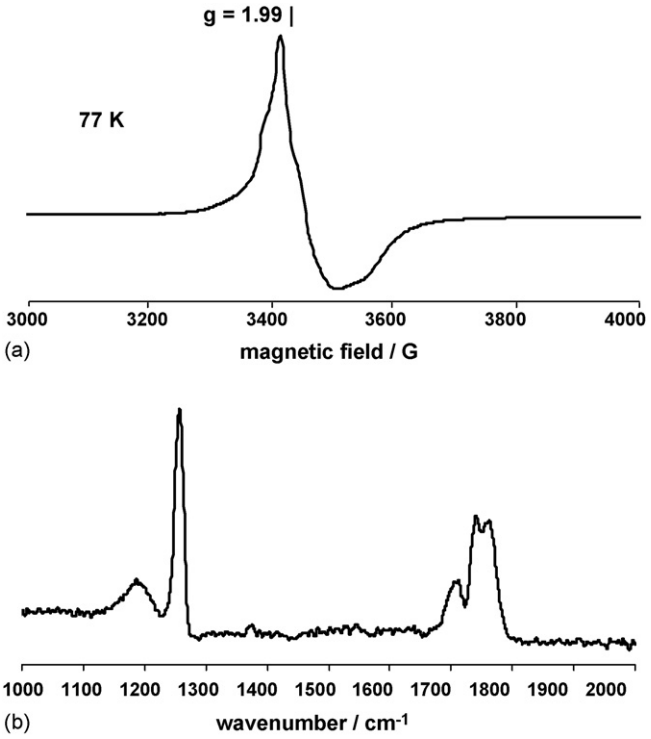

Fig. 4. EPR (a) and IR (b) spectra of $Ce_{0.10}Zr_{0.90}O_2$ system after NO_2 (20 Torr) adsorption at 77 K.

ascribed to $\delta(NO_2)$ vibrations in N_2O_4 dimers stabilized on the surface [29]. Weak maxima from surface nitrites occurring at ~1300 and 1255 cm^{-1} provide an additional evidence of NO_2 stabilization on the surface of ceria-rich CeO_2–ZrO_2 in the form of diamagnetic species. As in the previous case subsequent introduction of oxygen led to nitrate formation.

4. Conclusions

The CeO_2/ZrO_2 ratio controls the bulk structure and surface properties of $Ce_xZr_{1-x}O_2$ solid solutions. Increasing content of CeO_2 favors metastabilization of both tetragonal (t′ and t″) and cubic polymorphs, altering their reactivity toward NO and NO_2. Adsorption of NO on ceria-rich tetragonal ($P4_2/nmc$) solid solutions led to formation of mono- and dimeric nitrosyl complexes of various thermal stabilities. NO_2 decomposes only on ceria-lean monoclinic ($P2_1/c$) samples, whereas dimerization of NO_2 is preferred for samples with higher CeO_2 contents. The main products of NO_2 decomposition are surface nitrosyls and nitrates.

Acknowledgements

This work, carried out in the framework of the French-Polish collaboration within the *Jumelage* Program "*Materials for Environment*", was financially supported by The Polish State Committee for Scientific Research (KBN) within the project no. 3 T09 147 26. The authors are grateful to Dr. Aleksandra Wesełucha-Birczyńska from Regional Laboratory of Physicochemical Analyses and Structural Research for recording the

Raman spectra and to *RHODIA* for providing us kindly the CeO_2–ZrO_2 samples of various composition.

References

[1] J. Kašpar, P. Fornasiero, M. Graziani, Catal. Today 50 (1999) 285.
[2] P. Vidmar, P. Fornasiero, J. Kašpar, G. Gubitosa, M. Graziani, J. Catal. 171 (1997) 160.
[3] P. Fornasiero, G. Balducci, R. Di Monte, J. Kašpar, V. Sergo, G. Gubitosa, A. Ferrero, M. Graziani, J. Catal. 164 (1996) 173.
[4] A. Martínez-Arias, J. Soria, J.C. Conesa, X.L. Seoane, A. Arcoya, R. Cataluña, J. Chem. Soc. Faraday Trans. 91 (1995) 1679.
[5] P. Fornasiero, R. Di Monte, G. Ranga Rao, J. Kašpar, S. Meriani, A. Trovarelli, M. Graziani, J. Catal. 151 (1995) 168.
[6] A. Trovarelli (Ed.), Catalysis by Ceria and Related Materials, Imperial College Press, London, 2002.
[7] M. Daturi, C. Binet, J.C. Lavalley, G. Blanchard, Surf. Interf. Anal. 30 (2000) 273.
[8] E. Finocchio, M. Daturi, C. Binet, J.C. Lavalley, G. Blanchard, Catal. Today 52 (1999) 53.
[9] A. Volodin, D. Biglino, Y. Itgaki, M. Shiotani, A. Lund, Chem. Phys. Lett. 327 (2000) 165.
[10] E. Mamontov, R. Brezny, M. Koranne, T. Egami, J. Phys. Chem. B 107 (2003) 13007.
[11] E. Mamontov, T. Egami, R. Brezny, M. Koranne, S. Tyangi, J. Phys. Chem. B 107 (2003) 13007.
[12] M. Yashima, H. Arashi, M. Kakihana, M. Yoshimura, J. Am. Ceram. Soc. 77 (1994) 1067.
[13] T. Mitsuhashi, M. Ichihara, U. Tatsuke, J. Am. Ceram. Soc. 57 (1974) 97.
[14] M. Fernández-García, A. Martínez-Arias, J.C. Hanson, J.A. Rodriguez, Chem. Rev. 104 (2004) 4063.
[15] R.C. Garvie, J. Phys. Chem. 69 (1965) 1238.
[16] T. Spalek, P. Pietrzyk, Z. Sojka, J. Chem. Inf. Model. 45 (2005) 18.
[17] T. Hirata, E. Asari, M. Kitajima, J. Solid State Chem. 110 (1994) 201.
[18] V. Sánchez-Escribano, E. Fernández-López, M. Panizza, C. Resini, J.-M. Gallardo-Amores, G. Busca, Solid State Sci. 5 (2003) 1369.
[19] P. Fornasiero, A. Speghini, R. Di Monte, M. Bettinelli, J. Kašpar, A. Bigotto, V. Sergo, M. Graziani, Chem. Mater. 16 (2004) 1938.
[20] M.J. Torralvo, M.A. Alario, J. Soria, J. Catal. 146 (1994) 335.
[21] M. Figaj, K.D. Becker, Solid State Ionics 141/142 (2001) 507.
[22] M. Occhiuzzi, D. Cordischi, R. Dragone, J. Phys. Chem. B 106 (2002) 12464.
[23] J.A. McCleverty, J. Mol. Catal. 13 (1981) 309.
[24] P.C. Ford, I.M. Lorkovic, Chem. Rev. 102 (2002) 993.
[25] A. Volodin, D. Biglino, Y. Itgaki, M. Shiotani, A. Lund, Chem. Phys. Lett. 327 (2000) 165.
[26] A.A. Davydov, Infrared Spectroscopy of Adsorbed Species on the Surface of Transition Metal Oxides, John Wiley & Sons, Chichester, 1990 .
[27] A. Adamski, G. Djéga-Mariadassou, Z. Sojka, Catal. Today, (2006), in press.
[28] D. Astruc, Electron Transfer and Radical Processes in Transition-Metal Chemistry, Wiley, New York, 1995, p. 235.
[29] K.I. Hadjiivanov, Catal. Rev. Sci. Eng. 42 (2000) 71.
[30] H. Yahiro, A. Lund, R. Aasa, N.P. Benetis, M. Shiotani, J. Phys. Chem. A 104 (2000) 7950.
[31] H. Myiata, S. Konishi, T. Ohno, F. Hatayama, J. Chem. Soc. Faraday Trans. 91 (1995) 1557.
[32] M. Kantcheva, A.S. Vakkasoglu, J. Catal. 223 (2004) 352.
[33] M. Haneda, T. Morita, Y. Nagao, Y. Kintaishi, H. Hamada, PCCP 3 (2001) 4696.
[34] A.N. Il'ichev, G.A. Konin, V.A. Matyshak, A.M. Kuli-Zade, V.N. Korchak, Yu.B. Yan, Kinet. Catal. 43 (2002) 214.
[35] P.J. Schmitz, R.J. Baird, J. Phys. Chem. B 106 (2002) 4172.